

New constraints on radii and tidal deformabilities of neutron stars from GW170817

Elias R. Most,¹ Lukas R. Weih,¹ Luciano Rezzolla,^{1,2} and Jürgen Schaffner-Bielich¹

¹*Institut für Theoretische Physik, Max-von-Laue-Straße 1, 60438 Frankfurt, Germany*

²*Frankfurt Institute for Advanced Studies, Ruth-Moufang-Straße 1, 60438 Frankfurt, Germany*

We explore in a parameterized manner a very large range of physically plausible equations of state (EOSs) for compact stars for matter that is either purely hadronic or that exhibits a phase transition. In particular, we produce two classes of EOSs with and without phase transitions, each containing one million EOSs. We then impose constraints on the maximum mass, ($M < 2.16M_{\odot}$), and on the dimensionless tidal deformability ($\tilde{\Lambda} < 800$) deduced from GW170817, together with recent suggestions of lower limits on $\tilde{\Lambda}$. Exploiting more than 10^9 equilibrium models for each class of EOSs, we produce distribution functions of all the stellar properties and determine, among other quantities, the radius that is statistically most probable for any value of the stellar mass. In this way, we deduce that the radius of a purely hadronic neutron star with a representative mass of $1.4 M_{\odot}$ is constrained to be $12.00 < R_{1.4}/\text{km} < 13.45$ at a $2\text{-}\sigma$ confidence level, with a most likely value of $\bar{R}_{1.4} = 12.39$ km; similarly, the smallest dimensionless tidal deformability is $\tilde{\Lambda}_{1.4} > 375$, again at a $2\text{-}\sigma$ level. On the other hand, because EOSs with a phase transition allow for very compact stars on the so-called “twin-star” branch, small radii are possible with such EOSs although not probable, i.e., $8.53 < R_{1.4}/\text{km} < 13.74$ and $\bar{R}_{1.4} = 13.06$ km at a $2\text{-}\sigma$ level, with $\tilde{\Lambda}_{1.4} > 35.5$ at a $3\text{-}\sigma$ level. Finally, since these EOSs exhibit upper limits on $\tilde{\Lambda}$, the detection of a binary with total mass of $3.4 M_{\odot}$ and $\tilde{\Lambda}_{1.7} > 461$ can rule out twin-star solutions.

PACS numbers: 04.30.Db, 04.40.Dg, 95.30.Sf, 97.60.Jd 26.60Kp 26.60Dd 26.60Gj

Introduction. On August 17 2017, the Advanced LIGO and Virgo network of gravitational-wave detectors have recorded the signal from the inspiral of a binary neutron-star system, i.e., event GW170817 [1]. Less than a couple of seconds later, the gravitational-wave signal was followed by a series of electromagnetic emissions. These electromagnetic counterparts have provided the long-sought confirmation that merging neutron-star binaries can be associated with short gamma-ray bursts, shedding important light on the long-standing puzzle of the origin of these phenomena [2–5].

These multimessenger observations, together with numerical simulations of merging neutron stars (see [6, 7] for recent reviews), and the modelling of the kilonova emission from this process [8–10] have provided important new insight on the maximum mass of neutron stars and on the expected distribution in radii [11–17]. The approaches followed in these works differ significantly in the techniques employed, but provide a remarkably robust picture of what is the maximum mass of nonrotating stellar models M_{TOV} . For example, by combining the signal from GW170817 and quasi-universal relations (see, e.g., [18, 19]) that correlate M_{TOV} with the maximum mass supported through uniform rotation M_{max} [20] (see [21] for the case of differential rotation), Ref. [15] has set constraints on the maximum mass to be $2.01_{-0.04}^{+0.04} \leq M_{\text{TOV}}/M_{\odot} \lesssim 2.16_{-0.15}^{+0.17}$, where the lower limit comes from pulsar observations [22]. Similarly, by considering the most generic family of neutron-star-matter equations of state (EOSs) that interpolate between recent nuclear-physics results at low and high baryon densities, Ref. [11] has set constraints for the radius of a $1.4 M_{\odot}$ neutron star to be $R_{1.4} < 13.6$ km, while the minimum dimensionless tidal deformability is $\tilde{\Lambda}_{1.4} > 120$.

In this *Letter*, we reconsider the problem of constraining the radii and tidal deformability of neutron stars considering more than two million different EOSs (with and without a

phase transition) that are physically plausible and respect the observational constraints on the maximum mass. Using this large set of equilibria, we explore the distribution functions of stellar models and how they are affected by the imposition of various constraints, be them on the maximum mass or on the dimensionless tidal deformability.

Explorations of this type have been considered in the recent past, starting from the works of Refs. [23, 24] (see also [25]), who derived limits on the neutron-star radius by using data from X-ray binaries combined with parametrized EOSs (see [26, 27] for recent reviews). When compared with these approaches, our results benefit from several improvements. First, we impose, and in a differential manner, recent constraints on the maximum mass [13, 15–17] and on the tidal deformability [10, 14] coming directly from GW170817 and that obviously could not have been included by previous works, e.g., [23, 24, 28, 29]. Second, we exploit recent improvements on the EOS of neutron matter in the outer core [30], which plays a fundamental role in determining the stellar radius. Third, we carry out the first systematic study of the statistical properties of the tidal deformability highlighting that the lower limit for $\tilde{\Lambda}$ is very tightly constrained. Finally, we explore a more recent, but also more restricted, prescription for the outer core as infinite neutron matter [31] and compare to the results obtained using the setup employed by [11]. Hereafter, masses will be in units of solar masses and radii in kilometres.

Methods and setup We compute models of cold nonrotating neutron stars by numerically solving the Tolman-Oppenheimer-Volkoff (TOV) equations together with an EOS. As the complete EOS is unknown, we construct a parameterized set of EOSs by taking into account calculations that describe nuclear matter in the outer crust [32, 33], state-of-the-art descriptions of nuclear matter close to nuclear-saturation

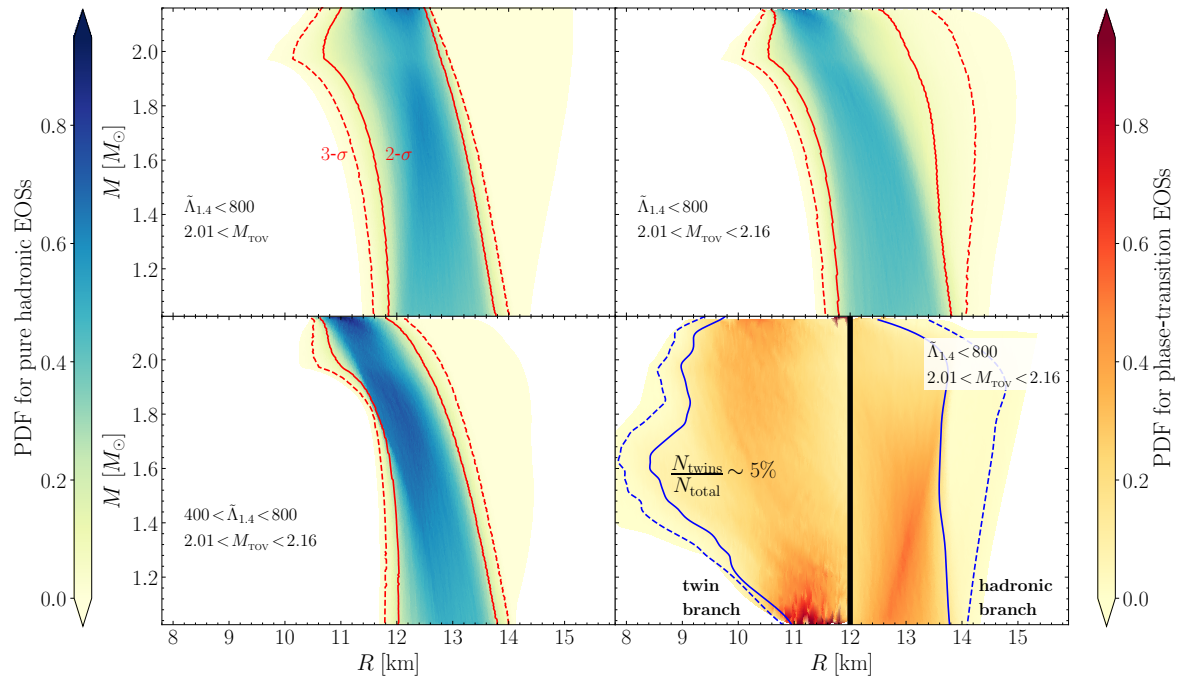


FIG. 1. PDFs of stellar radii. Top-left panel: PDF with only the observational constraints on the observed maximum mass and tidal deformability for pure hadronic EOSs; top-right: PDF when also an upper limit is set on the maximum mass; bottom-left: PDF with the combined constraints on maximum mass and tidal deformability; bottom-right: the same as in the bottom-left but for EOSs with a phase transition; the thick black line at 12 km distinguishes the PDFs of hadronic twin stars, which represent only 5% of the total sample with phase transitions. In all panels the solid and dashed lines indicate the 2- σ and 3- σ confidence levels, respectively.

density [30, 31], together with perturbative QCD calculation for matter at densities exceeding that in the core of neutron stars [34, 35]. Because the EOS at intermediate densities is not well known, we construct it using piecewise polytropes, overall following [36]. Additionally, we account for the existence of phase transitions by considering EOSs that admit a jump in the energy density between randomly chosen segments of the polytropes [29, 37–39], and thus allowing for “twin-star” solutions [40–42] (see the supplemental material for details [43]).

Radius and tidal deformability constraints. Figure 1 offers a complete view of the probability distribution functions (PDFs) built using our $\sim 2 \times 10^9$ stellar models. The top-left panel, in particular, shows the color-coded PDF when only the *observational* constraints are imposed on the maximum mass [22] and on the tidal deformability [1], i.e., $2.01 < M_{\text{TOV}}$ and $\tilde{\Lambda}_{1.4} < 800$ (see Fig. 3 of the supplemental material [43] for the PDF with only the maximum-mass constraint). Indicated with red solid and dashed lines are the values at which the corresponding cumulative distributions at fixed mass reach a value of 2- σ and 3- σ , respectively, thus setting both a minimum and a maximum value for the radius at that mass with a probability of $\sim 95\%$ and 99.7% . Note that the PDF extends beyond the red lines, but attains very small values in these regions. The top-right panel shows instead the PDF when, in addition to the lower limit, also an upper limit is set on the maximum mass i.e., $2.01 < M_{\text{TOV}} < 2.16$ [15], while keeping

the observational constraint on the tidal deformability. Note that the addition of this constraint changes the PDF, decreasing the average value of the maximum radius at a given mass. The bottom-left panel of Fig. 1 shows the impact of the combined observational and maximum mass constraints with that of a lower limit on the tidal deformability as suggested by Ref. [14], i.e., after considering $2.01 < M_{\text{TOV}} < 2.16$ and $400 < \tilde{\Lambda}_{1.4} < 800$. We note that although the constraint $\tilde{\Lambda}_{1.4} > 400$ set by Ref. [14] does not come with a systematic quantification of the uncertainties, it is reasonable that such a lower limit exists on the basis of the considerations made by Ref. [14].

The effect of these combined constraints is to significantly reduce the variance in the small-radii region and to refine the range for the most likely radii at a given mass. Note that the distribution now is not only restricted to a rather small range in radii, but it is also peaked around the small-radii end of the range. Because the EOS beyond nuclear-saturation density is not known, the possibility of phase transitions is also taken into account in the bottom-right panel, where we do not impose the $400 < \tilde{\Lambda}_{1.4}$ constraint since it is based on numerical simulation with EOSs without phase transitions. Furthermore, by splitting the panel at 12 km we distinguish between the PDF of the hadronic branch and the PDF of the “twin-star” branch, namely of all those stars that populate the small-radii second stable branch typical of models with a phase transition. Note that while the PDF on the hadronic branch is very

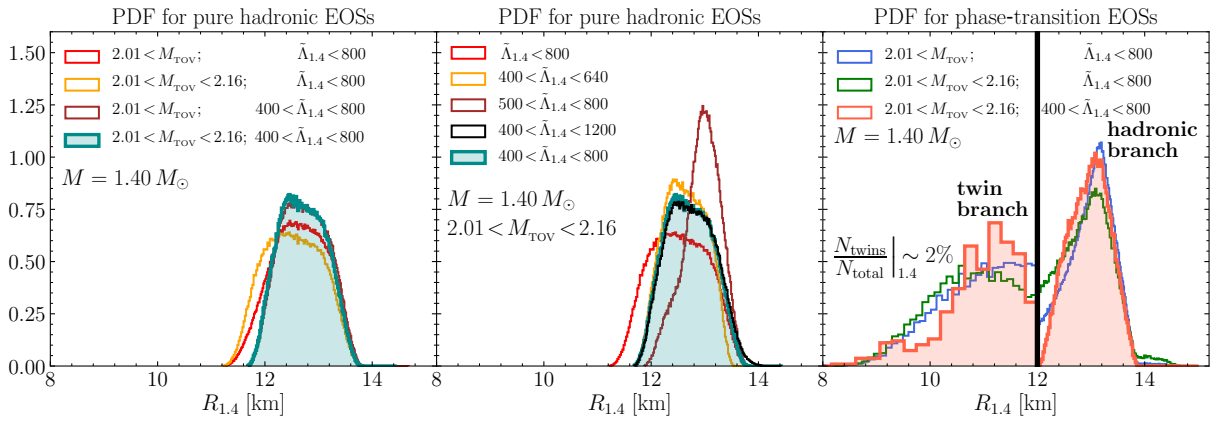


FIG. 2. PDFs of stellar radii for a neutron star with mass 1.4. Reported with different lines are the PDFs with different constraints on the maximum mass and tidal deformability (see legends); the left and middle panels refer to pure hadronic EOSs, while the right one to EOSs with a phase transition (cf. Fig. 1).

similar to the top-right panel, that of the twin-star branch is significantly different. In particular, we find that the radius varies in a much broader range, $8.53 < R_{1.4}/\text{km} < 13.74$, and is not as constrained as the hadronic branch; more importantly, the twin stars represent only $\sim 5\%$ of the total sample with phase transitions.

These last results are best appreciated when considering cuts of the bottom panels of Fig. 1 at a fixed value of the mass, e.g., 1.4. This is shown in the left panel of Fig. 2, which reports the PDF as a function of the radius at that mass, $R_{1.4}$. Shown with different lines are the distributions obtained when considering different constraints on the maximum mass or on the tidal deformability (see legend). Note that when only the observational constraints are imposed, either on the maximum mass or on the tidal deformability, the distribution functions are rather broad and flat, with a width of about almost three kilometres (cf. red and orange lines). On the other hand, when the combined distributions are considered, as shown with the green-shaded distribution, the variance decreases to about two kilometres and the PDF also exhibits a peak around the small-radii tail of the distribution. In this way, we are able to constrain $12.00 < R_{1.4} < 13.45$ at a $2\text{-}\sigma$ confidence level, with a most likely value of $\bar{R}_{1.4} = 12.45$. Although not shown in Fig. 2, we note that the PDFs are very robust upon changes in upper limit of the maximum mass, both when considering smaller (2.1) or larger (2.33) values for M_{TOV} . Conversely, the PDFs are rather sensitive to changes in $\tilde{\Lambda}$. This is illustrated in the middle panel of Fig. 2, which shows how the reference green-shaded PDF varies when, for $M = 1.4$ and $2.01 < M_{\text{TOV}} < 2.16$, different intervals are considered for the tidal deformability (see legend). Considering a large lower limit for the tidal deformability, e.g., from $\tilde{\Lambda}_{1.4} > 400$ to $\tilde{\Lambda}_{1.4} > 500$ (brown line), has the effect of excluding the softest EOSs and hence to shift the peak of the distribution to larger values, yielding a most likely value of $\bar{R}_{1.4} \simeq 13.0$ and a variance which is below 2 km. By contrast, changing the upper limit of the tidal deformability, e.g., taking the less con-

servative observational limit $\tilde{\Lambda}_{1.4} < 640$ [1] (orange line), or an even more conservative limit of $\tilde{\Lambda}_{1.4} < 1200$ (black line), does not change the distribution significantly.

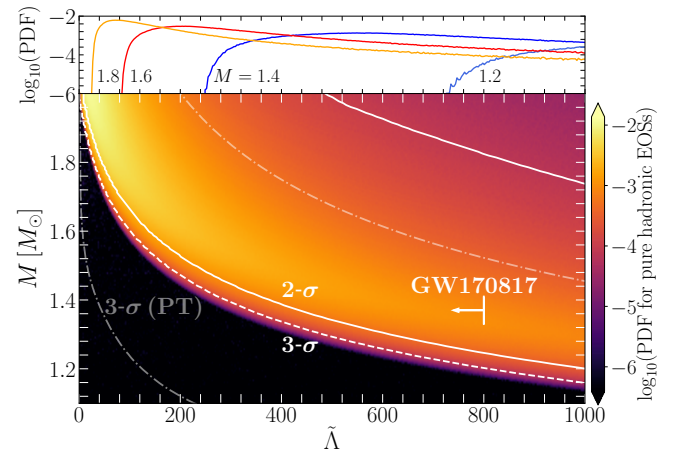


FIG. 3. PDF of the tidal deformability $\tilde{\Lambda}$ for pure hadronic EOSs satisfying the constraint $M_{\text{TOV}} > 2.01$. The white solid and dashed lines show where the corresponding cumulative distributions at fixed mass reach a value of $2\text{-}\sigma$ and $3\text{-}\sigma$, respectively. Also shown are the $3\text{-}\sigma$ regions for EOS featuring a phase transition. Shown with an arrow is the upper limit deduced from GW170817, while several cuts at fixed $\tilde{\Lambda}$ masses are shown in the top panel.

Finally, when considering the distribution of models with phase-transitions, the behaviour in the right panel of Fig. 2 is rather different. While the application of the combined maximum mass and $\tilde{\Lambda}_{1.4}$ constraints yields the same results presented in the left panel (green and orange shaded curves), with $\bar{R}_{1.4} = 13.06$ at a $2\text{-}\sigma$ level, the twin-star branch is much broader, i.e., $8.53 < R_{1.4} < 13.74$. Note that although small-radii stars are possible, they are not probable and that the twin-branch stars are only $\sim 2\%$ of the total sample with phase transition for $M = 1.4$. Also, note that if a constraint such as $\tilde{\Lambda}_{1.4} > 400$ could be applied to EOSs with phase transitions, it would only sharpen the mean value of the PDF for twin

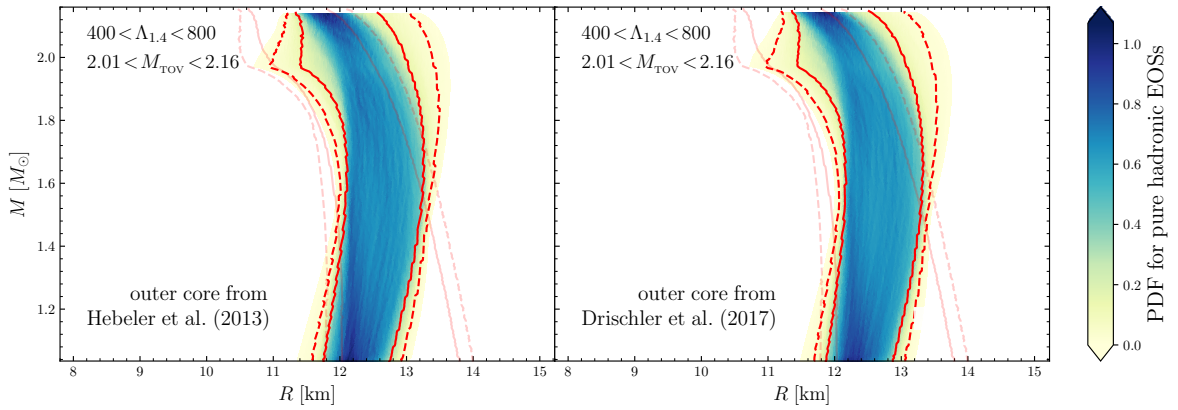


FIG. 4. *Left panel:* The same as in bottom-right panel of Fig. 1, but when the neutron matter in the outer core is treated following the approach of [44]. *Right panel:* The same as in the left panel but when considering the more recent prescription of [31] for the outer core. Shown as light shaded lines are the 2/3- σ values reported in the bottom-right panel of Fig. 1.

stars, but again exclude the small-radii models of the hadronic branch (orange curve).

Additional information on the tidal deformability is presented in Fig. 3, which reports the PDF of $\tilde{\Lambda}$ for the hadronic EOS, with again the white solid (dashed) lines showing where the corresponding cumulative distributions at fixed mass reach a value of 2- σ (3- σ). Furthermore, we indicate with grey dashed-dotted lines the 3- σ values for EOSs with a phase transition (cf. Fig. 4 of the supplemental material [43]). Shown instead with an arrow is the upper limit deduced from GW170817 [1]. The PDF in Fig. 3, which has not been presented before, points to three interesting properties. First, at any given mass the PDF is highly asymmetrical and has a very sharp cutoff in the lower-hand of the tidal deformability, which goes from $\tilde{\Lambda}_{\text{cutoff}} \sim 825$ at $M = 1.2$ to $\tilde{\Lambda}_{\text{cutoff}} \sim 285$ at $M = 1.4$ (see top panel of Fig. 3). Second, as the stellar mass increases, the distribution tends to a more pronounced peak and a smaller variance, with $0 \lesssim \tilde{\Lambda} \lesssim 480$ for $M = 2.0$. Finally, when considering a reference mass of 1.4, we can set $\tilde{\Lambda}_{1.4} > 375$ (290), again at a 2 (3)- σ confidence level, respectively. Similarly, the corresponding value for a 1.3 (1.5) mass becomes $\tilde{\Lambda}_{1.3(1.5)} > 615$ (230) at 2- σ . When allowing for phase-transitions we instead find that at 3- σ $\tilde{\Lambda}_{1.4} > 35.5$ and $\tilde{\Lambda}_{1.7} < 461$. Hence, a future gravitational-wave detection of a high-mass merger with a measured value of $\tilde{\Lambda}_{1.7} > 461$ can rule out twin stars below that mass. This is the first time that such upper limits have been provided on twin stars (see the supplemental material [43] for an extended discussion).

As a concluding but important remark, we illustrate in Fig. 4 the impact that different treatments of the outer core may have on the statistical properties of neutron star radii. In particular, the left panel of Fig. 4 shows the same distributions discussed in the bottom-left panel of Fig. 1 when following the treatment for the outer core discussed by Ref. [44], which is less conservative than the approach used here following Ref. [30]. Similarly, the right panel of Fig. 4 reports the corresponding distributions when the stellar models are built using

improved neutron-matter calculations [31]. Leaving aside the details of the two different calculations, it is interesting that estimates for the outer core that are only slightly less conservative yield tighter constraints for $R_{1.4}$, and a PDF with a smaller variance (the light-shaded red lines refer to [30]); in particular, we obtain a variance of ~ 1 km at a 2- σ level on the radii of low-mass stars. Figure 4 thus highlights that a more accurate knowledge of the matter in the outer core, i.e., for number densities in the range $0.08 \lesssim n/\text{fm}^{-3} \lesssim 0.21$, can have an enormous impact on the macroscopic properties of neutron stars. Any progress in this direction will impact our understanding of compact stars. For completeness we comment that while the results of [31] constrain the hadronic sector very well, we found their effect on the twin-star branch to be less pronounced.

Conclusions. Using a parameterized construction of the EOS which matches realistic nuclear-physics calculations for the stellar crust at very low densities and perturbative QCD calculations at very high densities, we have constructed more than two million different EOSs, with and without phase transitions, that are physically plausible and compatible with the observations on the maximum mass. The corresponding PDFs have been studied to set constraints on the plausible values for the radii and tidal deformabilities of neutron stars. In particular, we have studied how the PDFs are affected by the imposition of new constraints on the maximum mass and on the tidal deformability that have been recently deduced via GW170817. These additional constraints induce significant changes in the PDFs, especially when they are imposed simultaneously. While the statistical properties of the stellar models vary only weakly with the maximum mass, constrains on the lower limit of the tidal deformability exclude the softest EOSs and shift the peak of the distribution to larger values, yielding a variance well-below two kilometres for purely hadronic EOSs, i.e., $12.00 < R_{1.4} < 13.45$ at a 2- σ level, with a most likely value of $\bar{R}_{1.4} = 12.39$. On the other hand, the radii of twin stars are less constrained, namely, $8.53 < R_{1.4} < 13.74$,

with very compact stars possible but not probable, so that $\bar{R}_{1.4} = 13.06$. We have also been able to set upper limits on the tidal deformability of hybrid stars, e.g., $\tilde{\Lambda}_{1.7} < 461$. For hadronic EOSs an additional tightening of the uncertainties is achieved with refined descriptions of the outer core, thus calling for an improved characterisation of the EOS at intermediate densities. Overall, our results show that GW170817 has had a profound impact on our ability to constrain the maximum mass, tidal deformability and radii of neutron stars. New detections will provide even tighter constraints on the EOS of nuclear matter and restrict the radius of neutron stars to below the 10% uncertainty [45–48].

Acknowledgements. It is a pleasure to thank Christian Drischler, Arianna Carbone, Kai Hebeler, Jim Lattimer, Tyler Gorda and Alekski Vuorinen for useful discussions. Support comes from: “PHAROS”, COST Action CA16214; LOEWE-Program in HIC for FAIR; the DFG through the grant CRC-TR 211; the European Union’s Horizon 2020 Research and Innovation Programme (Grant 671698) (call FETHPC-1-2014, project ExaHyPE). ERM and LRW acknowledge support from HGS-HiRe.

-
- [1] B. P. Abbott *et al.* (LIGO Scientific Collaboration and Virgo Collaboration), *Phys. Rev. Lett.* **119**, 161101 (2017)
- [2] D. Eichler, M. Livio, T. Piran, and D. N. Schramm, *Nature* **340**, 126 (1989)
- [3] R. Narayan, B. Paczynski, and T. Piran, *Astrophys. J. Lett.* **395**, L83 (1992), [astro-ph/9204001](#)
- [4] L. Rezzolla, B. Giacomazzo, L. Baiotti, J. Granot, C. Kouveliotou, and M. A. Aloy, *Astrophys. J. Letters* **732**, L6 (2011), [arXiv:1101.4298 \[astro-ph.HE\]](#)
- [5] E. Berger, *Annual Review of Astron. and Astrophys.* **52**, 43 (2014), [arXiv:1311.2603 \[astro-ph.HE\]](#)
- [6] L. Baiotti and L. Rezzolla, *Rept. Prog. Phys.* **80**, 096901 (2017), [arXiv:1607.03540 \[gr-qc\]](#)
- [7] V. Paschalidis, *Classical and Quantum Gravity* **34**, 084002 (2017), [arXiv:1611.01519 \[astro-ph.HE\]](#)
- [8] L. Bovard, D. Martin, F. Guercilena, A. Arcones, L. Rezzolla, and O. Korobkin, *Phys. Rev. D* **96**, 124005 (2017), [arXiv:1709.09630 \[gr-qc\]](#)
- [9] B. D. Metzger, *Living Reviews in Relativity* **20**, 3 (2017), [arXiv:1610.09381 \[astro-ph.HE\]](#)
- [10] A. Perego, D. Radice, and S. Bernuzzi, *Astrophys. J. Lett.* **850**, L37 (2017), [arXiv:1711.03982 \[astro-ph.HE\]](#)
- [11] E. Annala, T. Gorda, A. Kurkela, and A. Vuorinen, ArXiv e-prints (2017), [arXiv:1711.02644 \[astro-ph.HE\]](#)
- [12] A. Bauswein, O. Just, H.-T. Janka, and N. Stergioulas, *Astrophys. J. Lett.* **850**, L34 (2017), [arXiv:1710.06843 \[astro-ph.HE\]](#)
- [13] B. Margalit and B. D. Metzger, *Astrophys. J. Lett.* **850**, L19 (2017), [arXiv:1710.05938 \[astro-ph.HE\]](#)
- [14] D. Radice, A. Perego, F. Zappa, and S. Bernuzzi, *Astrophys. J. Lett.* **852**, L29 (2018), [arXiv:1711.03647 \[astro-ph.HE\]](#)
- [15] L. Rezzolla, E. R. Most, and L. R. Weih, *Astrophys. J. Lett.* **852**, L25 (2018), [arXiv:1711.00314 \[astro-ph.HE\]](#)
- [16] M. Ruiz, S. L. Shapiro, and A. Tsokaros, *Phys. Rev. D* **97**, 021501 (2018), [arXiv:1711.00473 \[astro-ph.HE\]](#)
- [17] M. Shibata, S. Fujibayashi, K. Hotokezaka, K. Kiuchi, K. Kyutoku, Y. Sekiguchi, and M. Tanaka, *Phys. Rev. D* **96**, 123012 (2017), [arXiv:1710.07579 \[astro-ph.HE\]](#)
- [18] K. Yagi and N. Yunes, *Phys. Rep.* **681**, 1 (2017), [arXiv:1608.02582 \[gr-qc\]](#)
- [19] B. Haskell, R. Ciolfi, F. Pannarale, and L. Rezzolla, *Mon. Not. R. Astron. Soc. Letters* **438**, L71 (2014), [arXiv:1309.3885 \[astro-ph.SR\]](#)
- [20] C. Breu and L. Rezzolla, *Mon. Not. R. Astron. Soc.* **459**, 646 (2016), [arXiv:1601.06083 \[gr-qc\]](#)
- [21] L. R. Weih, E. R. Most, and L. Rezzolla, *Mon. Not. R. Astron. Soc.* **473**, L126 (2018), [arXiv:1709.06058 \[gr-qc\]](#)
- [22] J. Antoniadis, P. C. C. Freire, N. Wex, T. M. Tauris, R. S. Lynch, and et al., *Science* **340**, 448 (2013), [arXiv:1304.6875 \[astro-ph.HE\]](#)
- [23] F. Özel, G. Baym, and T. Güver, *Phys. Rev. D* **82**, 101301 (2010), [arXiv:1002.3153 \[astro-ph.HE\]](#)
- [24] A. W. Steiner, J. M. Lattimer, and E. F. Brown, *Astrophys. Journ.* **722**, 33 (2010), [arXiv:1005.0811 \[astro-ph.HE\]](#)
- [25] F. Özel and D. Psaltis, *Phys. Rev. D* **80**, 103003 (2009), [arXiv:0905.1959 \[astro-ph.HE\]](#)
- [26] J. M. Lattimer and M. Prakash, *Physics Reports* **621**, 127 (2016), [arXiv:1512.07820 \[astro-ph.SR\]](#)
- [27] F. Özel and P. Freire, *Annual Review of Astronomy and Astrophysics* **54**, 401 (2016), [arXiv:1603.02698 \[astro-ph.HE\]](#)
- [28] G. Hagen, A. Ekström, C. Forssén, G. R. Jansen, W. Nazarewicz, and et al., *Nature Physics* **12**, 186 (2016)
- [29] A. W. Steiner, C. O. Heinke, S. Bogdanov, C. Li, W. C. G. Ho, A. Bahramian, and S. Han, *Mon. Not. R. Astron. Soc.* (2018), [10.1093/mnras/sty215](#), [arXiv:1709.05013 \[astro-ph.HE\]](#)
- [30] C. Drischler, A. Carbone, K. Hebeler, and A. Schwenk, *Phys. Rev. C* **94**, 054307 (2016), [arXiv:1608.05615 \[nucl-th\]](#)
- [31] C. Drischler, K. Hebeler, and A. Schwenk, ArXiv e-prints (2017), [arXiv:1710.08220 \[nucl-th\]](#)
- [32] G. Baym, C. Pethick, and P. Sutherland, *Astrophys. J.* **170**, 299 (1971)
- [33] J. W. Negele and D. Vautherin, *Nuclear Physics A* **207**, 298 (1973)
- [34] A. Kurkela, P. Romatschke, and A. Vuorinen, *Phys. Rev. D* **81**, 105021 (2010), [arXiv:0912.1856 \[hep-ph\]](#)
- [35] E. S. Fraga, A. Kurkela, and A. Vuorinen, *Astrophys. J. Lett.* **781**, L25 (2014), [arXiv:1311.5154 \[nucl-th\]](#)
- [36] A. Kurkela, E. S. Fraga, J. Schaffner-Bielich, and A. Vuorinen, *Astrophys. J.* **789**, 127 (2014)
- [37] J. M. Lattimer and A. W. Steiner, *Astrophys. J.* **784**, 123 (2014), [arXiv:1305.3242 \[astro-ph.HE\]](#)
- [38] I. Tews, J. Carlson, S. Gandolfi, and S. Reddy, ArXiv e-prints (2018), [arXiv:1801.01923 \[nucl-th\]](#)
- [39] I. Tews, J. Margueron, and S. Reddy, ArXiv e-prints (2018), [arXiv:1804.02783 \[nucl-th\]](#)
- [40] M. G. Alford, S. Han, and M. Prakash, *Phys. Rev. D* **88**, 083013 (2013), [arXiv:1302.4732 \[astro-ph.SR\]](#)
- [41] D. E. Alvarez-Castillo and D. B. Blaschke, *Phys. Rev. C* **96**, 045809 (2017), [arXiv:1703.02681 \[nucl-th\]](#)
- [42] J.-E. Christian, A. Zacchi, and J. Schaffner-Bielich, *European Physical Journal A* **54**, 28 (2018), [arXiv:1707.07524 \[astro-ph.HE\]](#)
- [43] See Supplemental Material for details on the EOS and the impact of phase transitions, which includes Refs. [49, 50].
- [44] K. Hebeler, J. M. Lattimer, C. J. Pethick, and A. Schwenk, *Astrophys. J.* **773**, 11 (2013), [arXiv:1303.4662 \[astro-ph.SR\]](#)
- [45] L. Rezzolla and K. Takami, *Phys. Rev. D* **93**, 124051 (2016), [arXiv:1604.00246 \[gr-qc\]](#)
- [46] S. Bose, K. Chakravarti, L. Rezzolla, B. S. Sathyaprakash, and K. Takami, *Phys. Rev. Lett.* **120**, 031102 (2018),

- [arXiv:1705.10850 \[gr-qc\]](#)
- [47] K. Chatziioannou, J. A. Clark, A. Bauswein, M. Millhouse, T. B. Littenberg, and N. Cornish, *Phys. Rev. D* **96**, 124035 (2017), [arXiv:1711.00040 \[gr-qc\]](#)
 - [48] H. Yang, V. Paschalidis, K. Yagi, L. Lehner, F. Pretorius, and N. Yunes, *Phys. Rev. D* **97**, 024049 (2018), [arXiv:1707.00207 \[gr-qc\]](#)
 - [49] K. Hebeler, S. K. Bogner, R. J. Furnstahl, A. Nogga, and A. Schwenk, *Phys. Rev. C* **83**, 031301 (2011), [arXiv:1012.3381 \[nucl-th\]](#)
 - [50] S. De, D. Finstad, J. M. Lattimer, D. A. Brown, E. Berger, and C. M. Biwer, ArXiv e-prints (2018), [arXiv:1804.08583 \[astro-ph.HE\]](#)

SUPPLEMENTAL MATERIAL

Parameterizing our ignorance

In the following we give a detailed description of the construction of the EOS used in our work. In essence, for the low-density limit we use the EOSs of Refs. [1, 2], that describe the neutron star's crust up until a number density of $n_{\text{crust}} = 0.08 \text{ fm}^{-3}$. Instead, for baryon number densities n_{B} found in the outer core, i.e., between n_{crust} and $n_{\text{B}} \approx 1.3 n_{\text{sat}} \approx 0.21 \text{ fm}^{-3}$, where $n_{\text{sat}} = 0.16 \text{ fm}^{-3}$ is the nuclear-saturation density, we use an improved and consistent neutron-matter EOS based on the chiral expansion at N^3LO of the nucleon-nucleon and three-nucleon (3N) chiral interactions that takes into account also the subleading 3N interactions, as well as 4N forces in the Hartree-Fock approximation [3]. In practice, we take the lower and upper limits of the uncertainty band for this EOS and fit them with two polytropes. The first polytrope is used up until $\approx n_{\text{sat}}$ and yields an adiabatic index Γ_1 in the range [1.31, 1.58], while the second adiabatic index Γ_2 is chosen in the range [2.08, 2.38]; the limits of these ranges essentially establish the uncertainty in the description of the EOS in the outer core. We note that taking just these very stiff and soft limits into account – as done by Ref. [4] – only allows to give upper and lower bounds, as set by the softest and stiffest EOS possible. On the other hand, to understand common features and effects of the crust and outer core on the neutron-star models, we construct our EOSs from uniform distributions of Γ_1 and Γ_2 , which will obviously include the stiffest and softest possible EOSs, but also all the other possibilities between these two limits. In addition, and to explore the sensitivity of our results on this prescription of the EOS, we also investigate the impact of a further refinement of the EOS obtained using a new many-body Monte-Carlo framework for perturbative calculations applied to a set of chiral interactions [5]. In this case, we use the range over six EOSs, each based on a different Hamiltonian [6], as uncertainty band.

For the high-density part of the EOS, on the other hand, we follow [4] and [7], and use the cold quark-matter EOS derived by [8], which is based on the perturbative QCD calculation of [9]. The uncertainty in this EOS is estimated by changing the renormalization scale parameter within a factor two, $X \in [1, 4]$, which is chosen from a uniform distribution, allowing us to match the last segment of the interpolating piecewise polytrope via its adiabatic index at the baryon chemical potential $\mu_{\text{b}} = 2.6 \text{ GeV}$. Finally, for the unconstrained region above $\sim 1.3 n_{\text{sat}}$, we follow [7] and interpolate between these limits using piecewise polytropes with four segments (tetrapoles), whose polytropic exponents, as well as the matching points between the segments, are chosen at random assuming equal probabilities, ensuring continuity of energy and pressure at the matching points. We have also checked our results to be robust, when using five instead of four polytropic segments.

After constructing an EOS with the procedure outlined

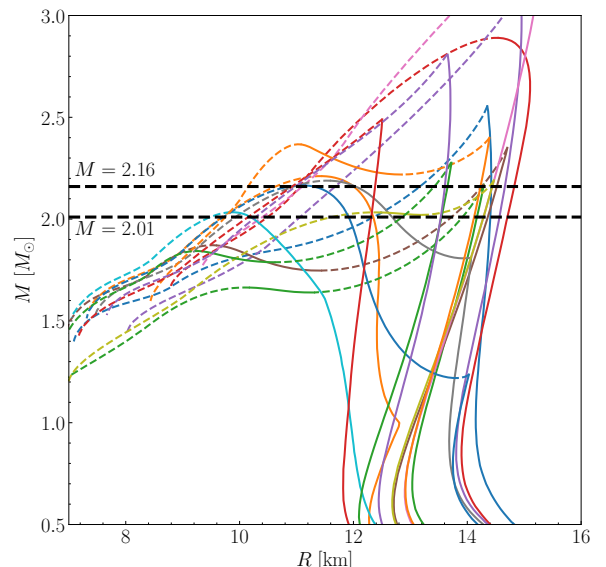


FIG. 1. Representative sample of (M, R) curves constructed from EOSs with a phase transition. While stable branches are shown as solid lines, the unstable ones are denoted by dashed ones. Also shown with thick dashed lines are the lower and upper constraint on the maximum mass.

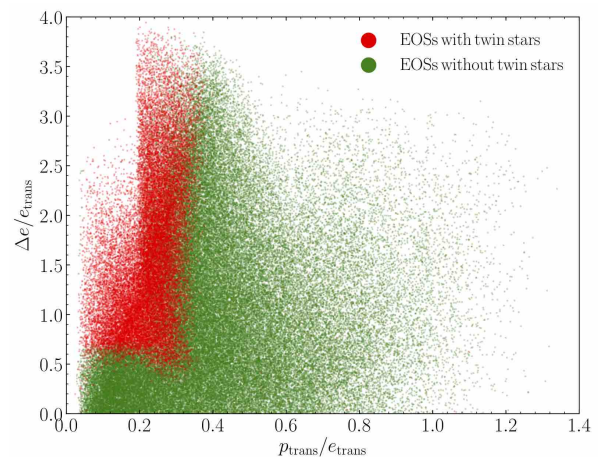


FIG. 2. Relative jump of the energy discontinuity $\Delta e/e_{\text{trans}}$ shown as a function of the normalised pressure at the phase transition $p_{\text{trans}}/e_{\text{trans}}$. All EOSs represented possess a phase transition but some lead to twin stars (red dots), while others do not (green dots).

above, we check that it is physically plausible by ensuring that the sound speed is subluminal everywhere inside the star, while the minimal thermodynamic stability criteria is automatically satisfied. For any EOS passing this test, we then construct a sequence of neutron-star models by solving the TOV equations. Additionally, we check compatibility with observations of the maximum mass of neutron stars [10] and ensure that the maximum mass of any sequence exceeds 2.01. In this way, we compute a million of equilibrium sequences containing more than a billion stars and essentially covering the whole possible range of EOSs from very soft to very stiff.

As mentioned in the main text, in order to take into account

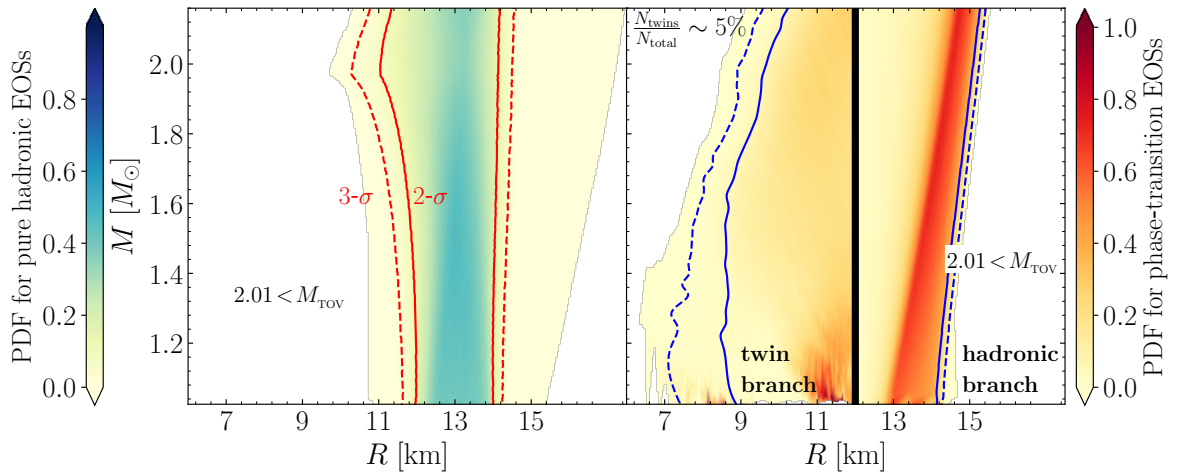


FIG. 3. PDFs of stellar radii. Left panel: PDF with only the observational constraints on the observed maximum mass for pure hadronic EOSs; right: the same but for EOSs with a phase transition and where the PDF for $R < 12$ km is for the twin-branch and the one for $R > 12$ km for the hadronic branch. In both panels the solid and dashed lines indicate the $2\text{-}\sigma$ and $3\text{-}\sigma$ confidence levels, respectively. This figure should also be contrasted with Fig. 1 of the main text.

the possibility that the neutron-star matter has a strong phase transition in its interior, we construct an equally sized set of 10^6 EOSs using the above setup, but adding a jump in energy density $\Delta e \in [0, 1000] \text{ MeV}/\text{fm}^3$, while ensuring constancy of the chemical potential. This jump is introduced randomly between the polytropic segments and its range is motivated by the results of Ref. [11]. The latter choice ensures that all four categories of twin stars can be obtained (see [11] for an overview). This is also evident from Fig. 1, which shows a representative sample of the mass radius-curves obtained with the setup for EOSs with phase transition. In particular, it is possible to see that the phase transition can set in at very low masses, i.e., $< 1 M_\odot$, but also at very high masses, i.e., $> 3 M_\odot$, where the two stable branches can be up to 5 km apart. Overall, we find that with this prescription we can cover well the space of possible EOSs with a phase transition.

A more detailed representation of the occurrence and properties of the phase transitions in the EOSs constructed here can be obtained by looking at Fig. 2, which shows the relative length of the jump $\Delta e/e_{\text{trans}}$ over $p_{\text{trans}}/e_{\text{trans}}$, where p_{trans} is the pressure at the onset of the phase transition and e_{trans} the corresponding energy. The figure clearly shows that our sample of EOSs with phase transitions populates the whole space necessary for obtaining all four categories of twin stars (cf. Fig. 3 of Ref. [11]). The red region also confirms that twin stars can only be obtained for a small set of combinations of the parameters Δe and e_{trans} . Additionally, we can see that the remaining parameter space is also covered well.

Comparing EOSs with and without phase transitions

While purely hadronic EOSs yield neutron star-models with radii $\gtrsim 10$ km, this is not contradicting the results of Ref. [12], who also find models with radii as small as ~ 8 km.

From Fig. 3, where we show all models without any upper constraint on the maximum mass and the tidal deformabilities, it is evident that such small radii can only be obtained when a phase transition is present. At the same time, it is evident that such compact stars are not likely and require some fine-tuning of the EOS. For instance, we find that such small radii are found for twin stars, whose total number, N_{twins} , only corresponds to $\sim 5\%$ of the total number of all models build from EOS exhibiting a phase transition, N_{total} .

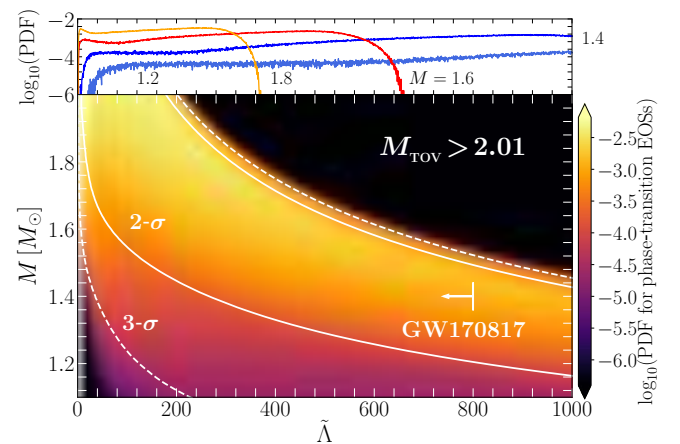


FIG. 4. The same as Fig. 3 of the main text, but for the set of EOSs with phase transition.

Another striking difference between purely hadronic EOSs and the ones with phase transitions is the occurrence of small tidal deformabilities in the latter case. For instance, for $M \lesssim 1.4$ models with $\tilde{\Lambda}_{1.4} \lesssim 100$ can be found, as is evident from Fig. 4, which is the same as Fig. 3 of the main text but in the case of EOSs with a phase transition. This finding resolves the apparent conflict between the small lower limit for $\tilde{\Lambda}_{1.4}$ found in Ref. [13] (i.e., $\tilde{\Lambda}_{1.4} > 75$) and the stricter one obtained

by Ref. [4] (i.e., $\tilde{\Lambda}_{1.4} > 120$) or the value of $\tilde{\Lambda}_{1.4} > 375$ discussed in the main text. In the case of Ref. [13], in fact, no distinction was made between purely hadronic and EOSs with phase transitions. On the other hand, a comparison between Figs. 3 of the main text and 4 clearly shows that the lower limit on $\tilde{\Lambda}_{1.4}$ becomes much stricter if one assumes a purely hadronic EOS. A similar conclusion has been drawn in Ref. [12], where a model with phase transitions ($\tilde{\Lambda}_{1.4} > 80$) and one without ($\tilde{\Lambda}_{1.4} > 280$) was employed. In addition, we find that for $M \gtrsim 1.6$ a strict cut-off for the upper limit of $\tilde{\Lambda}$ exists if a phase transition is present. As a result, deducing a value of $\tilde{\Lambda}$ from a gravitational-wave measurement in this mass range could be used to distinguish a purely hadronic EOS from one with a phase transition, as we have further outlined in the main text.

-
- [1] G. Baym, C. Pethick, and P. Sutherland, *Astrophys. J.* **170**, 299 (1971)
 - [2] J. W. Negele and D. Vautherin, *Nuclear Physics A* **207**, 298 (1973)
 - [3] C. Drischler, A. Carbone, K. Hebeler, and A. Schwenk, *Phys. Rev. C* **94**, 054307 (2016), [arXiv:1608.05615 \[nucl-th\]](#)
 - [4] E. Annala, T. Gorda, A. Kurkela, and A. Vuorinen, ArXiv e-prints (2017), [arXiv:1711.02644 \[astro-ph.HE\]](#)
 - [5] C. Drischler, K. Hebeler, and A. Schwenk, ArXiv e-prints (2017), [arXiv:1710.08220 \[nucl-th\]](#)
 - [6] K. Hebeler, S. K. Bogner, R. J. Furnstahl, A. Nogga, and A. Schwenk, *Phys. Rev. C* **83**, 031301 (2011), [arXiv:1012.3381 \[nucl-th\]](#)
 - [7] A. Kurkela, E. S. Fraga, J. Schaffner-Bielich, and A. Vuorinen, *Astrophys. J.* **789**, 127 (2014)
 - [8] E. S. Fraga, A. Kurkela, and A. Vuorinen, *Astrophys. J. Lett.* **781**, L25 (2014), [arXiv:1311.5154 \[nucl-th\]](#)
 - [9] A. Kurkela, P. Romatschke, and A. Vuorinen, *Phys. Rev. D* **81**, 105021 (2010), [arXiv:0912.1856 \[hep-ph\]](#)
 - [10] J. Antoniadis, P. C. C. Freire, N. Wex, T. M. Tauris, R. S. Lynch, and et al., *Science* **340**, 448 (2013), [arXiv:1304.6875 \[astro-ph.HE\]](#)
 - [11] J.-E. Christian, A. Zacchi, and J. Schaffner-Bielich, *European Physical Journal A* **54**, 28 (2018), [arXiv:1707.07524 \[astro-ph.HE\]](#)
 - [12] I. Tews, J. Margueron, and S. Reddy, ArXiv e-prints (2018), [arXiv:1804.02783 \[nucl-th\]](#)
 - [13] S. De, D. Finstad, J. M. Lattimer, D. A. Brown, E. Berger, and C. M. Biwer, ArXiv e-prints (2018), [arXiv:1804.08583 \[astro-ph.HE\]](#)